Epiplakin Is Dispensable for Skin Barrier Function and for Integrity of Keratin Network Cytoarchitecture in Simple and Stratified Epithelia

Daniel Spazierer,[1]† Peter Fuchs,[1]† Siegfried Reipert,[1] Irmgard Fischer,[1] Matthias Schmuth,[2] Hans Lassmann,[3] and Gerhard Wiche[1]*

Department of Molecular Cell Biology, Max F. Perutz Laboratories, University of Vienna, 1030 Vienna, Austria[1]; Department of Dermatology and Venereology, Medical University of Innsbruck, 6020 Innsbruck, Austria[2]; and Center for Brain Research, Medical University of Vienna, 1090 Vienna, Austria[3]

Epiplakin, a giant epithelial protein of >700 kDa, belongs to the plakin family of cytolinker proteins. It represents an atypical family member, however, as it consists entirely of plakin repeat domains but lacks any of the other domains commonly shared by plakins. Hence, its putative function as a cytolinker protein remains to be shown. To investigate epiplakin's biological role, we generated epiplakin-deficient mice by gene targeting in embryonic stem cells. Epiplakin-deficient mice were viable and fertile, without developing any discernible phenotype. Ultrastructurally, their epidermis revealed no differences compared to wild-type littermates, and cornified envelopes isolated from skin showed no alterations in shape or stability. Furthermore, neither embryonal formation nor later function of the epithelial barrier was affected. In primary cultures of epiplakin-deficient keratinocytes, the organization of actin filaments, microtubules, and keratin networks was found to be normal. Similarly, no alterations in keratin network organization were observed in simple epithelia of small intestine and liver or in primary hepatocytes. We conclude that, despite epiplakin's abundant and highly specific expression in stratified and simple epithelia, its absence in mice does not lead to severe skin dysfunctions, nor has it detectable consequences for keratin filament organization and cytoarchitecture of cells.

The plakin family of cytolinker proteins comprises multidomain proteins, some of very large size (>500 kDa), that interconnect cytoskeletal filaments and anchor them at plasma membrane-associated adhesive junctions (for recent reviews, see references 18 and 28). Among the family members known to date are plectin, a versatile cytolinker that can interact with tubulin, actin, and intermediate filament networks; desmoplakin, a component of intercellular junctions; bullous pemphigoid antigen 1 (BPAG1), a hemidesmosomal plaque-associated plakin; ACF7/MACF, a microtubule-actin cross-linking factor; envoplakin and periplakin, both constituents of the cornified envelope (CE); and epiplakin, the most recently identified plakin. Structural features shared by several of these proteins include an amino-terminal actin-binding domain, a highly conserved plakin domain, a central coiled-coil or spectrin repeats-containing rod domain, and one or more usually C-terminal repeat domains, called plakin repeat domains (PRDs). The structural characteristics of epiplakin (M_r ~725) are exceptional, as it consists entirely of PRDs, 16 in case of the mouse (33). In accordance with their importance in maintaining tissue integrity and stability, genetic diseases affected by functional impairment of plakin proteins are often accompanied by skin blistering and other types of tissue fragility, such as muscular dystrophy and neuropathies (36).

A variety of genetically modified mouse models and spontaneous mutants have been studied to learn more about the functions of plakins. Desmoplakin knockout mice exhibited

embryonic lethality at day 6.5, resulting from defects in extraembryonic endoderm (11). Similarly, ACF7-deficient mice were reported to die during early embryonic development (20). Disruption of the plectin gene in mice led to the death of the animals 2 to 3 days after birth, most likely due to their severe skin blistering (3). Spontaneous deletions in the mouse BPAG1 gene cause an autosomal recessive neuropathy called dystonia musculorum (dt) (5). At the age of 1 to 2 weeks, homozygous *dt* mice display progressive loss of limb coordination caused by degeneration of sensory neurons, and the mice often die before weaning. Genetically altered mice that carry a BPAG1 null mutation show fragility of the skin upon mechanical stress in addition to the neuronal defect described for *dt* mice (12). Ablation of the envoplakin gene led to a greater proportion of immature CEs compared to wild-type mice and to some minor delay in the acquisition of the skin barrier function (23). Interestingly, targeted inactivation of periplakin did not reveal detectable abnormalities in the mouse (1). Animal models for epiplakin deficiencies have not been reported to date.

Epiplakin was classified as a plakin based on the sequence analysis of human and mouse cDNA (10, 33). Its multiple PRDs make it an attractive model for studying the functions of this domain. However, lacking any of the other structural motifs characteristic of plakins and consisting exclusively of PRDs, epiplakin must be considered as an atypical family member. Therefore, its relation to other plakin protein family members based on function remains to be investigated. On the transcript level, epiplakin was shown to be restricted to epithelial tissues (33), with highest expression found in skin. The more prominent expression of epiplakin in suprabasal compared to basal epidermal keratinocytes (33) may indicate a role of the protein

---

* Corresponding author. Mailing address: Department of Molecular Cell Biology, University of Vienna, Dr. Bohrgasse 9, A-1030 Vienna, Austria. Phone: 43 1 4277 52852. Fax: 43 1 4277 52854. E-mail: gerhard .wiche@univie.ac.at.
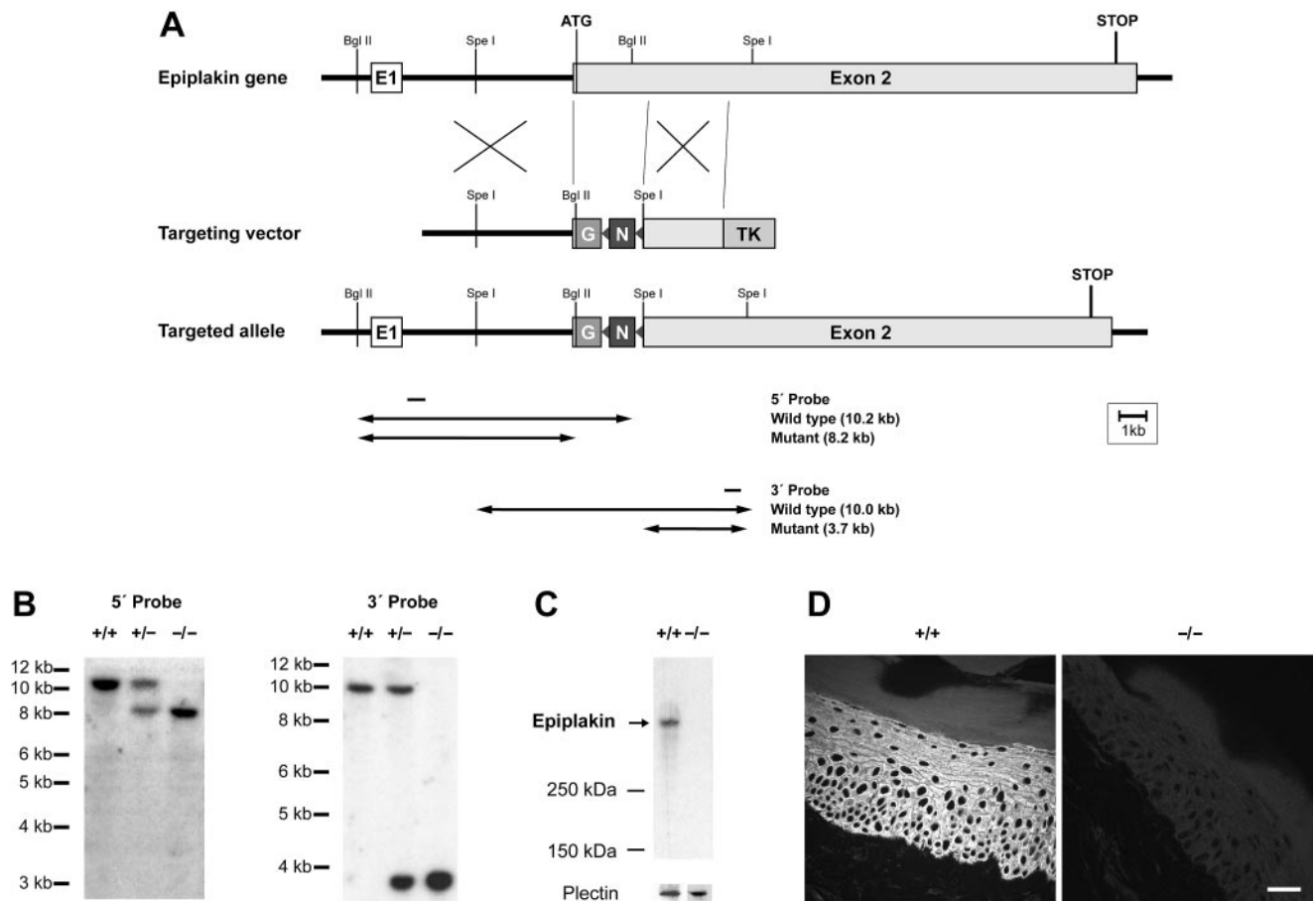
† D.S. and P.F. contributed equally to this work.

FIG. 1. Targeted inactivation of epiplakin. (A) Schematic representation of the epiplakin gene locus, the targeting vector, and the targeted allele. A total of 2,697 bp of epiplakin exon 2 were replaced by an in-frame GFP-encoding sequence (G) and a subsequent floxed neomycin resistance cassette (N). For negative selection, a thymidine kinase cassette (TK) was included at the 3′ end of the vector. Digestion of genomic DNA with the restriction enzyme BglII released 10.2-kb and 8.2-kb fragments from the wild-type and mutant alleles, respectively; with the restriction enzyme SpeI corresponding fragments of 10.0 kb and 3.7 kb were produced. Both alleles were detectable by 5′ (BglII digest) and 3′ (SpeI digest) external probes, as indicated. (B) Southern blot analysis of genomic DNA prepared from tail biopsies of wild-type (+/+), heterozygous (+/−), and knockout (−/−) mice using both (5′ and 3′) probes. DNA length standards are indicated. (C) Immunoblotting (3.75% polyacrylamide gel) of protein extracts from livers of epiplakin$^{+/+}$ and epiplakin$^{-/-}$ mice, using antibodies to epiplakin (upper part) and (after stripping of membranes) antibodies to the N terminus of plectin (lower panel; only relevant parts of blot are shown). Size markers are indicated in the upper panel. (D) Immunolocalization of epiplakin on frozen skin sections from adult wild-type (+/+) and epiplakin-deficient (−/−) mice using anti-epiplakin antibodies (33). Bar, 20 μm.

in skin barrier function, as suggested for other plakins (23, 34), especially as epiplakin fragments in preparations from the inner root sheath of the hair follicle were found to become cross-linked via transglutaminase 1 with trichohyalin, keratin, small prolin-rich protein, and involucrin (35). Recently, binding of one of the C-terminal repeat domains of epiplakin to keratin was demonstrated by blot overlay assay (17), and by knocking down epiplakin expression with RNA interference (RNAi), a collapse of keratin filaments was shown to take place in HeLa, but not in HaCaT or NHEK, cells (17). We report here the phenotypic analysis of epiplakin-deficient mice generated by targeted inactivation of the gene. Surprisingly, such mice showed a normal development, and no differences in morphology or functions of skin compared to wild-type littermates were detectable.

MATERIALS AND METHODS

All experiments involving animals were performed in accordance with Austrian Federal Government laws and regulations.

Construction of the targeting vector. In the targeting vector, the first 2,697 bp of epiplakin exon 2 (33) were replaced by an in-frame green fluorescent protein (GFP) gene and a subsequent thymidine kinase promoter-driven floxed neomycin resistance cassette (kindly provided by M. Kraus, Institute for Genetics, University of Cologne, Cologne, Germany). This minigene was flanked by 5.5 kb (5′) and 2.9 kb (3′) of epiplakin sequences for homologous recombination, and an herpes simplex virus thymidine kinase cassette (gift from E. Wagner, IMP, Vienna, Austria) was included at the 3′ end of the vector for negative selection.

Targeting of ES cells and generation of knockout mice. The linearized targeting vector was electroporated into embryonic day 14.1 (E14.1) embryonic stem (ES) cells, and G418- and ganciclovir-resistant colonies of cells heterozygous for the correctly targeted allele were isolated (15) and identified by Southern blot analysis (31). Germ line chimeras were obtained as previously described (15) and bred to C57BL/6 females to obtain F_1 mice heterozygous for the epiplakin deletion. Genotyping of offspring was performed by Southern blot analysis of tail DNA by digestion with BglII (5′ probe) and SpeI (3′ probe), respectively, and hybridization to two ^{32}P-labeled probes located outside of the homology arms (Fig. 1A and B).

Antibodies. The following primary antibodies were used: affinity-purified rabbit antibodies to epiplakin (raised against a recombinant fragment of mouse epiplakin containing the linker between modules 15 and 16) (33); antiserum to an N-terminal domain of plectin (N-term) (2); antiserum to C6-cell plectin (37);

rabbit antiserum TD2 to periplakin (23); rabbit antiserum 50K160 to keratins 8/18 (16); monoclonal antibodies (MAbs) to human BPAG1 (MAb-5E) (13), keratin 5 (AF 138; Covance, Princeton, NJ), keratins 5/6/18 (clone LP34; Dako-Cytomation, Glostrup, Denmark), tubulin (clone B-5-1-2; Sigma), actin (clone AC40; Sigma), involucrin (PRB-140C; Covance), and desmoplakin (clones DP-2.15, DP-2.17, and DP-2.20; Progen, Heidelberg, Germany); and a combination of commercially available MAbs to keratins 8 and 18 (clone Ks 8.7 and Ks 18.04; Progen). Specific applications are indicated in the figure legends. Secondary antibodies were purchased from Jackson Immuno-Research Laboratories (West Grove, PA).

Immunoblotting and immunohistochemistry. For immunoblotting, tissue homogenates were prepared from newborn mice by mechanical disruption as previously described (9). Proteins were separated by sodium dodecyl sulfate (SDS)-polyacrylamide gel electrophoresis (21), transferred to nitrocellulose sheets (Schleicher and Schuell, Dassel, Germany), and visualized as previously described (33).

For immunofluorescence microscopy, selected tissues were shock frozen in isopentane, cooled with liquid N_2, sectioned on a cryomicrotome, and fixed with acetone at $-20°C$. Sections (2 μm) were incubated with primary antibodies as specified.

Isolation of primary cells, cell culture, and immunofluorescence microscopy. Primary keratinocytes were isolated from 2- to 3-day-old mice as described previously (14). In short, epidermis was separated from dermis by trypsination for 18 h, minced, and stirred in a trypsinizing flask containing keratinocyte growth medium (KGM) (BioWhittaker, Rockland, ME) supplemented with 8% fetal calf serum (FCS) and 1.3 mM $CaCl_2$ for 30 min at 4°C. The cell suspension was filtered through a sterile Nytex gauze (40 μm) to remove the stratum corneum. Cells were sedimented at 800 rpm for 5 min, resuspended in KGM containing 2% FCS and 0.1 mM $CaCl_2$, and plated at relatively high density onto dishes coated with an 804G matrix (22). After attachment of keratinocytes (approximately 10 min), plates were washed twice with phosphate-buffered saline (PBS), and cells were grown in KGM.

For the isolation of primary hepatocytes, livers from E12.5 mouse fetuses were mechanically dissociated and plated onto plastic dishes in Dulbecco's modified Eagle's medium containing 10% FCS (8). Cells were washed with 1× PBS buffer, fixed in methanol for 90 s at $-20°C$, and washed three times with PBS. Dishes were blocked with 4% bovine serum albumin in PBS for 60 min. Thereafter, the samples were washed once with 0.05% Tween in PBS, incubated with primary antibodies for 60 min, and washed twice with PBS–0.05% Tween. After being washed, samples were incubated with secondary antibodies for 60 min and washed as before. The slides were mounted in Mowiol (Hoechst, Frankfurt, Germany) and examined using a Zeiss fluorescence laser-scanning microscope 510. Digital images were processed using Adobe Photoshop and Adobe Illustrator software.

Preparation of CEs and sonication experiments. Filtration remnants (stratum corneum) from the keratinocyte isolation procedure were boiled for 20 min in 2% SDS, 20 mM Tris-HCl, pH 7.5, 5 mM EDTA, and 10 mM dithiothreitol. CEs were sedimented at 5,000 rpm for 5 min and washed twice in 4 to 5 volumes of 0.2% SDS, 20 mM Tris-HCl, pH 7.5, 5 mM EDTA, and 10 mM dithiothreitol. Finally, CEs were resuspended in 2 volumes of the same solution and stored at 4°C. For disruption assays, CEs were sonicated in a Transsonic T780/H sonicator (Elma, Singen, Germany) for various lengths of time at room temperature.

Dye exclusion assay. Embryos were incubated for 1 min in 25, 50, and 75% methanol in PBS, followed by a 1-min incubation in 100% methanol, and a descending series of incubations in 75, 50, and 25% methanol in PBS for 1 min. Embryos were then washed in PBS for 1 min and stained with 0.1% toluidine blue O (Sigma, St. Louis, MO) for 10 min. After staining, embryos were embedded in agarose and photographed using a Nikon Coolpix 4500 digital camera. Images were processed with Adobe Photoshop, and the agarose background was removed.

Tape stripping, TEWL, and skin hydration measurements. Hair was removed from the back of adult mice by shaving 2 days prior to measuring transepidermal water loss (TEWL) on a 1.13-cm^2 area using an Evaporimeter (ServoMed, Stockholm, Sweden). TEWL values were registered in $g/m^2/h$ after equilibration of the probe on the skin (>60 s). Environment-related variables at the time of the study were an ambient air temperature of 21.5 to 22.3°C and an ambient air humidity of 30 to 34%. TEWL was measured both under basal conditions as well as following acute barrier disruption by repeated cellophane tape stripping, as previously described (32). Barrier recovery kinetics were then assessed by measuring TEWL at 4, 8, 24, and 48 h after acute disruption. For calculating percent change in TEWL, the following formula was used: [(TEWL stripped area at indicated time/TEWL control area at indicated time)/(TEWL stripped area before stripping/TEWL control area before stripping) -1] × 100. Stratum cor-

neum hydration was assessed as alterations in electrical capacitance (arbitrary units) using a corneometer (CM 825; Courage and Khazaka, Cologne, Germany).

Transmission electron microscopy. Adult mice were fixed by perfusion with 2.5% paraformaldehyde and 0.5% glutaraldehyde in PBS, pH 7.5, at 37°C via intercardiac puncture. Pieces of skin from the soles of mice were dissected and immersion fixed with 3% glutaraldehyde in Sorensen's buffer at 4°C overnight. Postfixation was done in 1.5% OsO_4 for 90 min, followed by dehydration in ethanol. Infiltration with epoxy resin (Agar 100) was performed in an electron microscopy tissue processor (Leica Microsystems, Austria).

Mouse skin was frozen using an EMPACT high-pressure freezer (Leica) as described in detail elsewhere (26). In short, adult mice were sacrificed by cervical dislocation, and skin samples were taken from their soles. The skin was dissected into pieces of about 0.3 mm^2, which were then transferred into flat specimen holders. Freezing occurred at a pressure of $2,005 \times 10^5$ Pa. After samples were frozen, they were transferred into an AFS freeze-substitution system (Leica) and substituted in 2% OsO_4 in acetone for 4 days at $-90°C$, followed by gradual warming, washing in anhydrous acetone, and infiltration with epoxy resin. Resin-infiltrated tissues were finally transferred to embedding molds filled with Agar 100 resin for polymerization at 60°C. Thin sections were cut with an Ultracut S ultramicrotome (Leica), mounted on copper grids, counterstained with uranyl acetate and lead citrate, and examined at 60 kV in a JEOL JEM-1210 electron microscope.

RESULTS

Gene targeting of epiplakin reveals no severe skin phenotype. To inactivate the epiplakin gene, a targeting vector was constructed in which the first 2,697 bp following the start codon of the gene were replaced by an expression cassette comprising a promotorless reporter gene (enhanced GFP) and neomycin resistance and thymidine kinase genes for positive/negative selection of ES cells (Fig. 1A). The neomycin resistance gene was flanked by *loxP* sites to enable its later deletion by Cre recombinase. ES cell clones selected were screened by Southern blot analysis using external 5′ and 3′ probes (Fig. 1A). From two of three independent clones injected into C57BL/6 blastocysts, we obtained germ line transmission of the targeted allele, as demonstrated by genomic Southern blotting (Fig. 1B, and data not shown).

To confirm the absence of epiplakin on the protein level, liver homogenates prepared from epiplakin$^{+/+}$ and epiplakin$^{-/-}$ mice were subjected to immunoblotting using highly potent antibodies to epiplakin (33). As shown in Fig. 1C, no immunoreactive bands were detected in samples from epiplakin$^{-/-}$ mice, while a single epiplakin band was stained in those from wild-type mice (Fig. 1C). Stripping and reprobing the blots with an antiserum to plectin confirmed comparable loading and transfer of proteins (Fig. 1C, lower panel). Furthermore, when cryosections of footpad skin were analyzed by immunofluorescence microscopy, no epiplakin was detected in samples from $-/-$ mice, while $+/+$ controls showed the typical staining pattern of epiplakin throughout all epidermal layers (Fig. 1D) (33).

Homozygous epiplakin-deficient mice were viable and showed no striking phenotypic alterations in comparison to heterozygous or wild-type littermates. Litter sizes from breedings of heterozygotes were comparable to those of wild-type animals, and genotyping of the viable offspring revealed normal Mendelian ratios. Epiplakin-deficient mice were fertile and produced normal litter sizes. Furthermore, no alterations in hair structure, hair subtype distribution, or hair cycle and morphogenesis could be detected in epiplakin$^{-/-}$ mice (data
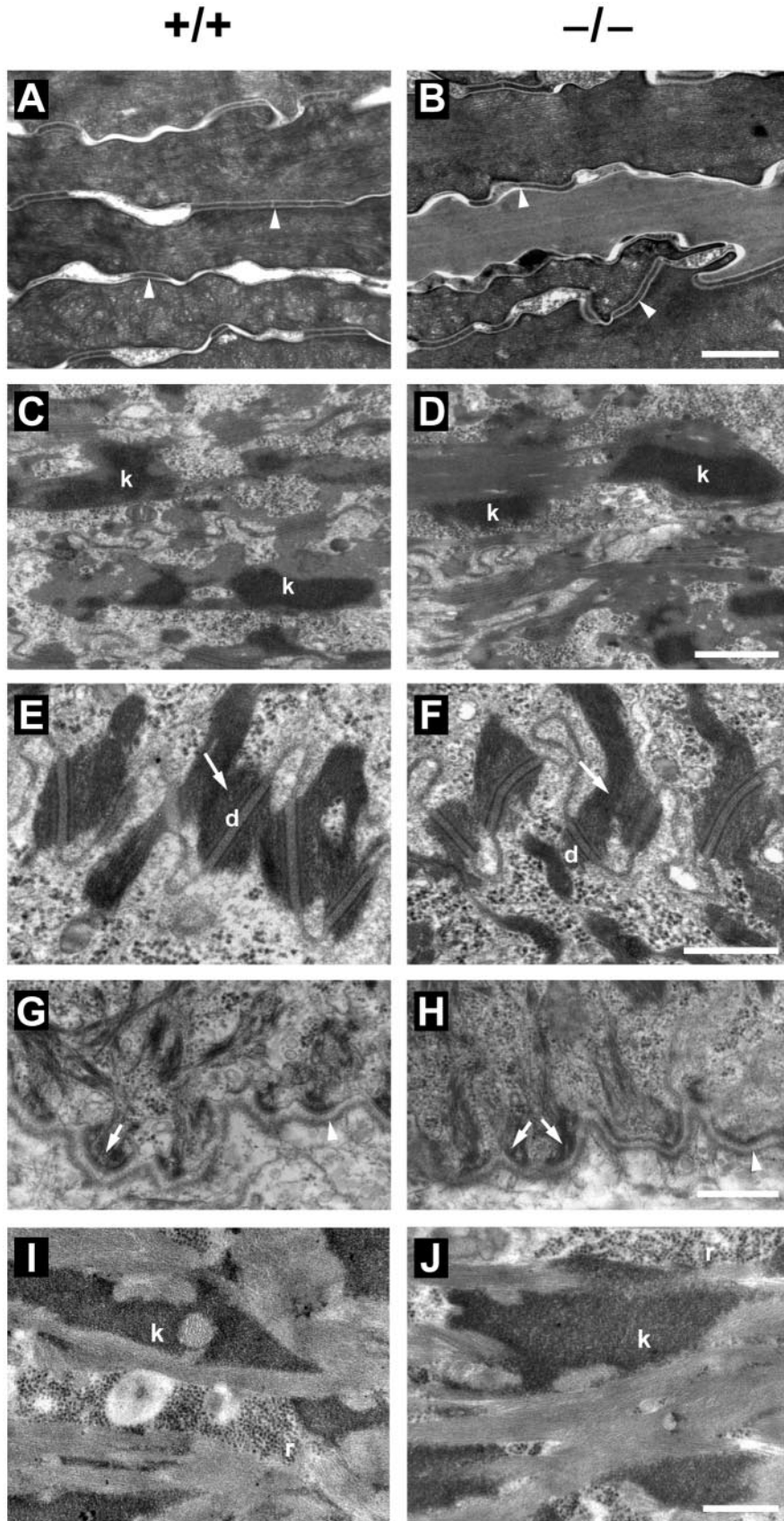
not shown), indicating that the hair coat of these mice was unaffected.

Considering that epiplakin is mainly expressed in skin (33), a more detailed ultrastructural analysis of this tissue seemed appropriate. Therefore, epoxy resin-embedded sections of the footpad skin from epiplakin$^{-/-}$ mice and epiplakin$^{+/+}$ littermates were inspected by transmission electron microscopy (Fig. 2). Desmosomes (Fig. 2E and F) and hemidesmosomes (Fig. 2G and H), both known to contain various plakins (18), showed no structural differences. Importantly, the depletion of epiplakin did not affect their association with keratin filament bundles, and hemidesmosomes were incorporated into structurally intact basal membranes (Fig. 2G and H). Suprabasal cell layers displayed typical features of cellular tissue undergoing terminal differentiation. In particular, the stratum granulosum contained, typically, densely packed bundles of keratin filaments and keratohyalin, with no differences found between epiplakin$^{+/+}$ and epiplakin$^{-/-}$ mice (Fig. 2C and D). When the tissue was subjected to high-pressure cryoimmobilization to better resolve the substructure of keratin filament bundles, laterally aligned individual filaments embedding keratohyalin structures could clearly be visualized. However, again no differences in the appearance of filaments became detectable between +/+ and −/− skin (Fig. 2I and J). Furthermore, in both wild-type and epiplakin-deficient skin, epidermal differentiation resulted in an ultrastructurally unaltered stratum corneum endowed with corneodesmosomes (Fig. 2A and B).

Intact CEs and unaltered expression levels and distribution of epidermal proteins in epiplakin$^{-/-}$ mice. Epiplakin has been proposed to serve a function in the outermost layers of the skin, especially in CEs (35). To reveal any changes in structure and/or stability of CEs inflicted by epiplakin deficiency, we isolated CEs from skin of newborn epiplakin-deficient and B6 wild-type mice. In a first comparison by phase-contrast microscopy, mixtures of angular and balloon-shaped envelopes were observed in both preparations without any apparent differences (Fig. 3A). Similarly, when the resistance of isolated CEs toward disruption through sonication was assessed, no differences between wild-type and epiplakin-deficient CEs could be detected (data not shown). To determine whether the expression levels of other CE proteins were changed in mice lacking epiplakin, proteins extracted from the skin of wild-type and epiplakin-deficient mice (two each) were analyzed by immunoblotting. With tubulin as a loading control, no significant difference could be found in the levels of involucrin, which is one of the main structural components of the CE (27) that was also found to be cross-linked to epiplakin in the inner root sheath of hair follicles (35), and of periplakin, another plakin located in the CE (30) (Fig. 3B); in the anti-epiplakin control lanes, no protein bands other than full-length
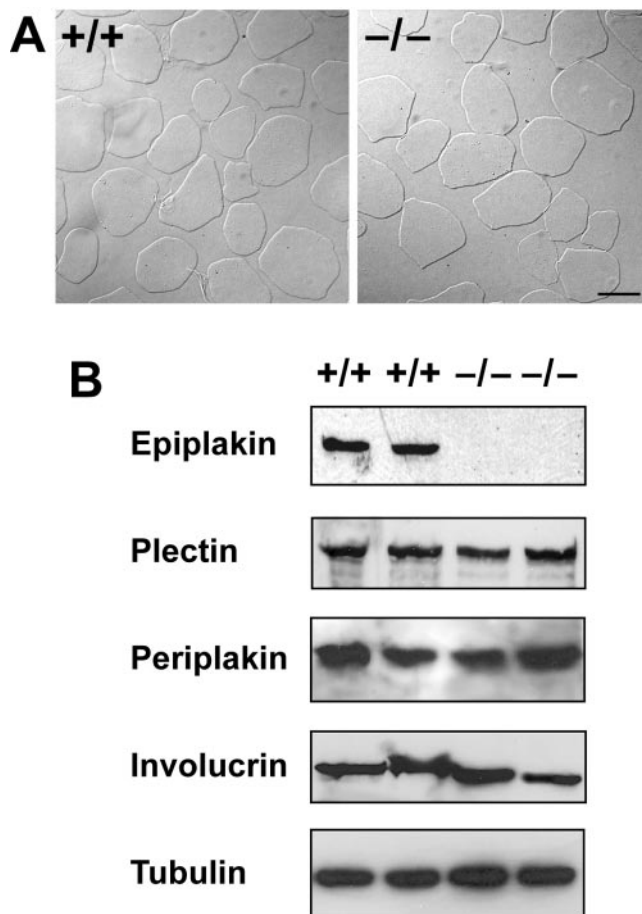

FIG. 3. Light microscopy of cornified envelopes (A) and expression profiles of epidermal proteins monitored by immunoblotting (B). (A) Note that CEs extracted from the skin of 1- to 3-day-old wild-type (+/+) and epiplakin-deficient (−/−) mice were indistinguishable from one another; angular and balloon-shaped envelopes were observed in both populations. Bar, 50 μm. (B) Protein extracts from skin of wild-type (+/+) and epiplakin-deficient (−/−) mice were subjected to immunoblotting using antibodies to epiplakin, plectin (N-term), periplakin, involucrin, and, as a loading control, tubulin. Only relevant parts of the blots are shown. Note that no significant differences in protein levels were observed when extracts obtained from wild-type and epiplakin-deficient mice (2 each) were compared.

epiplakin were detected (Fig. 3B and data not shown). We also tested whether the lack of epiplakin was compensated for by an upregulation of plectin, which is the closest relative of epiplakin within the plakin family and, like epiplakin, is expressed in all epidermal layers (33, 38). However, in this case again,

FIG. 2. Transmission electron microscopy of wild-type skin (A, C, E, G, and I) and epiplakin-deficient mouse footpad skin (B, D, F, H, and J). (A and B) Stratum corneum containing corneodesmosomes (arrowheads). (C and D) Stratum granulosum showing black keratohyalin granules (k) and contrasting keratin filament bundles, which appear gray. (E and F) Desmosomes (d) are structurally unaltered and characteristically associated with keratin bundles (arrows). (G and H) Basal membrane (arrowheads) mounted with hemidesmosomes (arrows) and associated keratin filaments. (I and J) High-pressure cryoimmobilized stratum granulosum. Both wild-type (I) and epiplakin-deficient tissues (J) display massive accumulations of orderly, aligned keratin filaments filling large areas of the granular cell layer. (k), keratohyalin embedded in the filamentous network. Note also ribosomes (r). Bars, 500 nm (B, F, H, and J) and 1 μm (D).
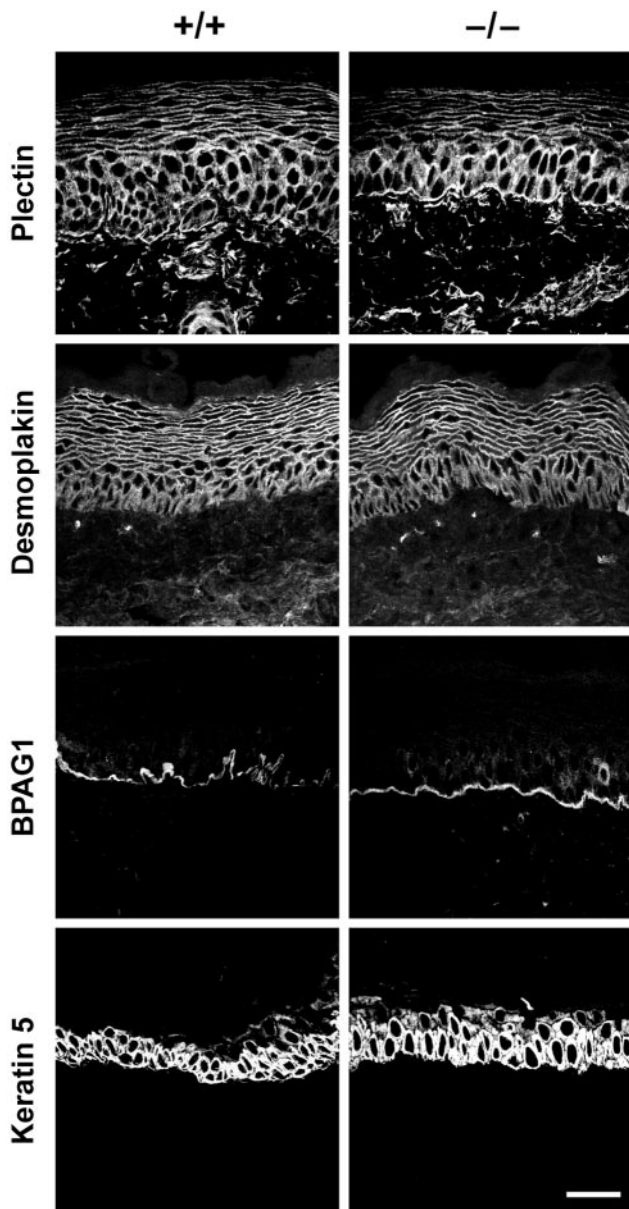
FIG. 4. Unaltered localization of epidermal proteins in epithelial cell layers of epiplakin-deficient mouse skin. Frozen skin sections from wild-type and epiplakin-deficient mice were subjected to immunofluorescence microscopy using antibodies to plectin (37), desmoplakin, BPAG1, and keratin 5 (AF138). Bar, 20 μm.

similar levels of the protein were found in wild-type and epiplakin-deficient mice (Fig. 3B).

Next, we investigated, whether epiplakin deficiency had any effect on other epidermal proteins, in particular their distribution to the various cell layers of skin and their intracellular localization. For this, cryosections obtained from footpad skin of epiplakin$^{+/+}$ and epiplakin$^{-/-}$ mice were subjected to immunofluorescence microscopy using antibodies to plectin, desmoplakin, periplakin, and BPAG1 (Fig. 4 and data not shown). However, in a comparison of both genotypes, hardly any differences in the staining patterns of these proteins were observed (Fig. 4). In both cases, plectin was detected in all cell

layers of the epidermis, with pronounced staining of the basement membrane; desmoplakin typically was associated with peripheral cell-cell junctions; and BPAG1 was associated with hemidesmosomes of basal epithelial cells. As there is evidence that epiplakin binds to keratins (17), it was also of interest to monitor the localization of keratins 5 and 10. In both epiplakin$^{+/+}$ and epiplakin$^{-/-}$ mice, keratin 5 expression was restricted to the basal layers of keratinocytes, while keratin 10 was found in the suprabasal layers of the epidermis (Fig. 4 and data not shown). Thus, neither expression nor localization of any of the epidermal proteins tested appeared to be altered in epiplakin-deficient mice. We also investigated the localization of keratin 6 in epiplakin$^{-/-}$ mice. In normal skin, keratin 6 is only expressed in hair follicle keratinocytes, but in traumatized skin it serves as a stress marker for interfollicular epidermis (24, 29). We found keratin 6 expression to be restricted to hair follicles without any detectable staining of the interfollicular epidermis (data not shown).

Normal embryonal development and functioning of the skin barrier in epiplakin-deficient mice. Even if CEs isolated from mutant mice seemed to be intact, it was still possible that the barrier function of skin was compromised in these mice. Therefore, we monitored epithelial barrier formation during their embryonic development using a dye exclusion assay. After backcrossing to the C57BL/6 wild-type strain for at least five generations to eliminate variations due to differences in genetic background, heterozygous epiplakin mice were used for breeding, and embryos were stained with toluidine blue at days E15.5 to E17.5. Until E16.5, neither epiplakin-deficient nor heterozygous nor wild-type mice had developed the skin barrier, while at E17.5 or later, all types of embryos showed a fully functional epithelial barrier against dye penetration (Fig. 5). Between stage E16.5 and stage E17.5, we found the dye being excluded from the dorsal surface first, without any detectable differences in acquisition patterns of mice that were $-/-$, $+/+$, or $+/-$ for epiplakin.

To determine whether the skin barrier function was still intact in adult epiplakin$^{-/-}$ animals, 2-month-old epiplakin-deficient mice and their wild-type littermates were subjected to TEWL measurements (4), a standard method to test the ability of the skin to prevent fluids from escaping into air. In addition, we assessed cohesion of the stratum corneum by measuring TEWL and the amount of protein removed after serial tape strippings (7). Both measurements give standard values correlating with corneocyte adhesion. The data obtained in this series of experiments were similar for both genotypes, indicating that there was no loss of barrier function in adult mutant mice (Fig. 6A and data not shown). Additionally, we measured TEWL within 48 h after tape stripping to test the ability of the skin to recover its water loss barrier function. These experiments, too, did not reveal any significant differences between wild-type and epiplakin-deficient litters (Fig. 6B). As an additional method suitable for testing the epithelial barrier, we measured skin hydration through surface electrical capacitance using a corneometer (39). Again, no phenotype was revealed, as epiplakin-deficient and control littermate mice showed similar levels of hydration (Fig. 6C).

Intact cytoarchitecture of epiplakin-deficient keratinocytes. To assess any alterations in network organization of major cytoskeletal filament systems in epiplakin-deficient cell cul-
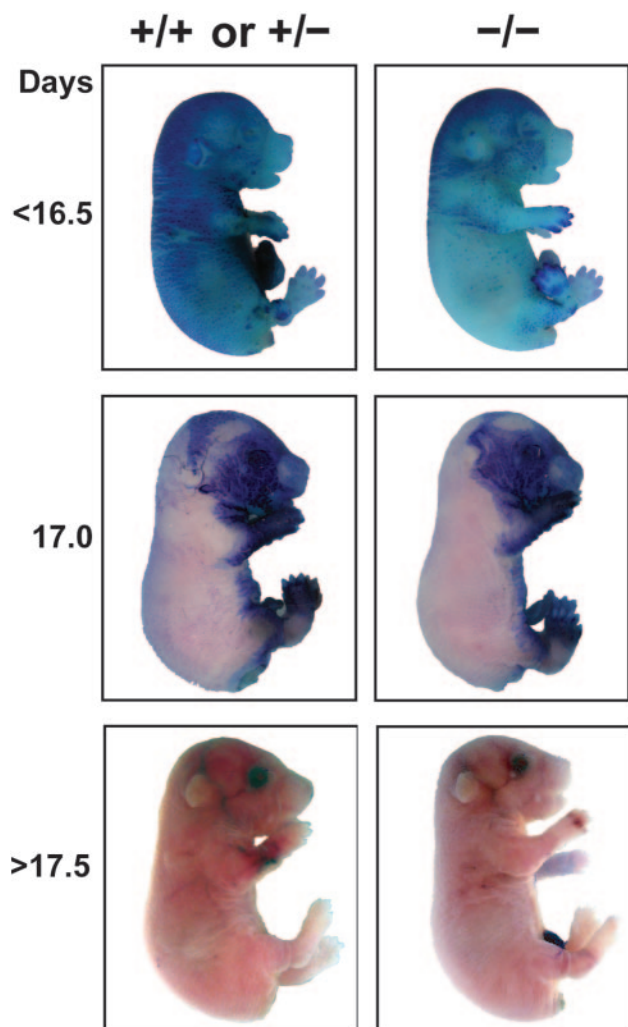
FIG. 5. Normal acquisition of epithelial barrier function during embryogenesis of epiplakin$^{-/-}$ mice. Dye (toluidine blue) exclusion assays were performed using embryos generated by epiplakin heterozygous breeders. For each embryonal time point (<E16.5, E17.0, and >E17.5) one representative embryo of either the wild-type (+/+) or heterozyous (+/−) and the homozygous mutant (−/−) genotype is shown.
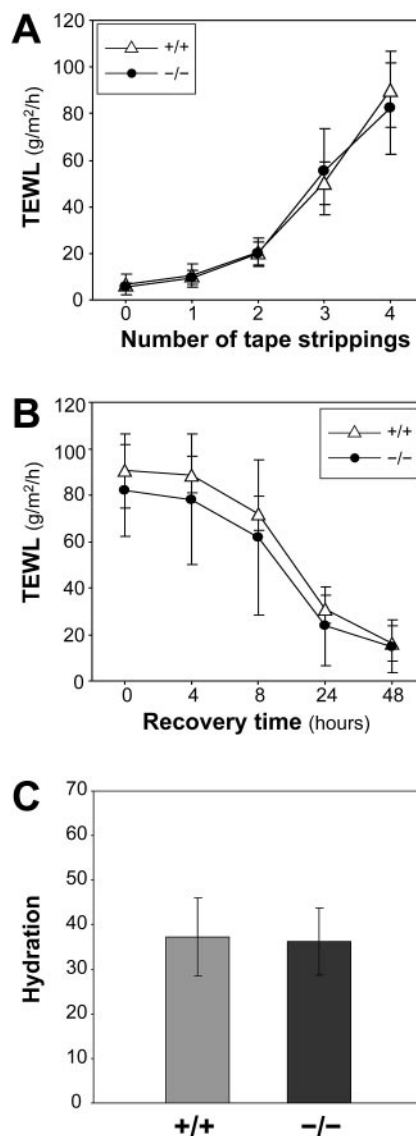

FIG. 6. Intact epithelial barrier function in adult epiplakin-deficient mice. (A) TEWL after serial tape strippings of skin of epiplakin-deficient mice and wild-type littermates. Basal TEWL (time zero) was measured before the first stripping. Mean TEWL ± standard deviation of five littermate pairs is shown after each of four tape strippings. (B) Recovery of epithelial barrier after tape stripping. Mean TEWL ± standard deviation of five littermate pairs of epiplakin$^{+/+}$ and epiplakin$^{-/-}$ mice was measured 4, 8, 24, and 48 h after final tape stripping. Note that TEWL was reduced to basal values within 48 h. (C) Hydration of stratum corneum of epiplakin-deficient mice and wild-type littermates measured with a corneometer. Mean values ± standard deviations of five littermate pairs are shown.

tures, primary keratinocytes were isolated from 1- to 3-day-old epiplakin$^{-/-}$ and corresponding epiplakin$^{+/+}$ control mice. Immunofluorescence microscopy using antibodies to tubulin revealed a dense, radial filamentous meshwork typical of microtubules in both wild-type and epiplakin-deficient cells (Fig. 7). Similarly, visualization of actin structures showed no difference between wild-type and epiplakin-deficient cells, both containing prominent stress fibers of particularly high density at the cell borders (Fig. 7). Finally, keratin filament networks also appeared to be normal in both types of cells (Fig. 7), consistent with the transmission electron microscopy data of high-pressure cryoimmobilized skin (Fig. 2I and J). Thus, epiplakin deficiency did not seem to effect any major changes in cytoarchitectural features of filament networks in keratinocytes. In addition, when the migratory ability of epiplakin-deficient keratinocytes was analyzed in a scratch wound assay,

no differences between mutant and wild-type control cells were observed (data not shown).

Normal keratin network organization in epiplakin-deficient simple epithelia. Using epiplakin RNA knockdown experiments, Jang et al. (17) reported a disruption of keratin filaments in HeLa cells but not in epidermal cells. This led the authors to speculate that epiplakin might play an important role in the organization and/or maintenance of keratin filaments in simple epithelia but not in stratified epithelia such as
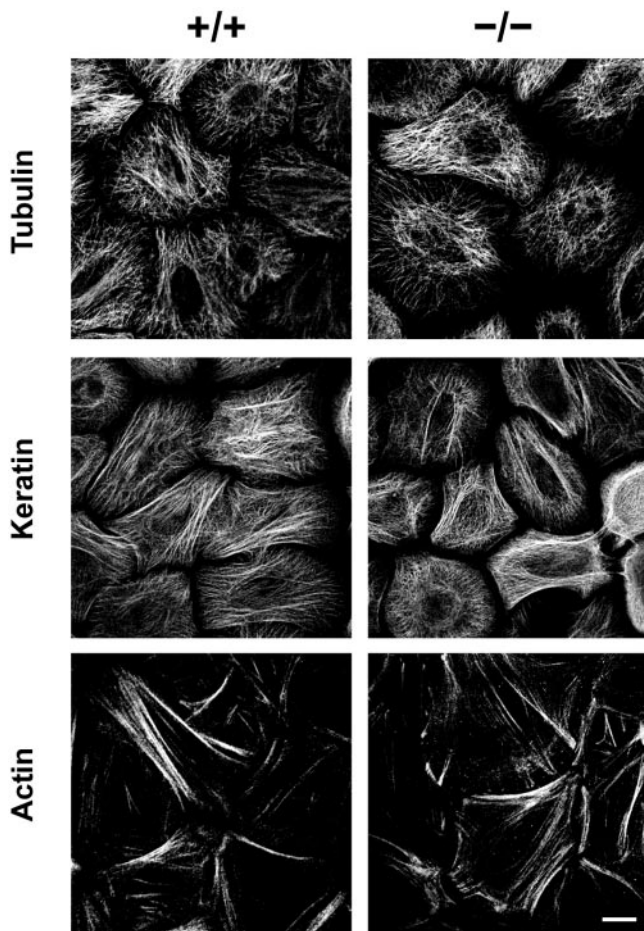
FIG. 7. Immunofluorescence microscopy of primary keratinocytes isolated from wild-type (+/+) and mutant (−/−) mice. Primary antibodies to tubulin, keratin (LP34), and actin were used. Bar, 10 μm.
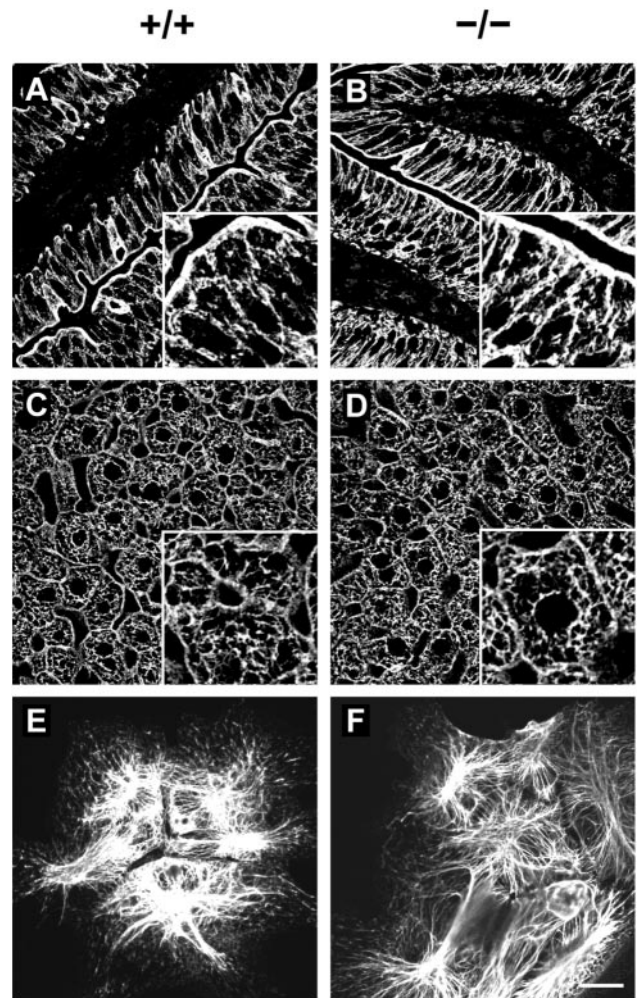

FIG. 8. Visualization of intact keratin filament networks in epiplakin-deficient simple epithelial tissues and primary cell cultures. Cryosections of small intestine (A and B) and liver (C and D) and primary hepatocytes isolated from fetal liver (E and F) of wild-type (+/+) and epiplakin-deficient (−/−) mice were subjected to immunofluorescence microscopy using antibodies to keratins 8 and 18 (50K160 for tissue sections; K_s 8.7 and K_s 18.04 for primary hepatocytes). Squares in lower-right-hand corners of panels A to D show ~2.5-fold magnifications of selected areas to demonstrate intactness of keratin filaments. Bar, 20 μm.

skin. However, when we visualized keratin filament networks in cryosections of small intestine and liver using antibodies to K8/K18, no differences between epiplakin-deficient and wild-type control tissues were apparent (Fig. 8A to D). Similarly, when primary hepatocytes isolated from the livers of epiplakin-deficient and wild-type control mice were subjected to immunofluorescence microscopy using a combination of antibodies to K8 and K18, intact and indistinguishable keratin network systems were visualized in both types of cells (Fig. 8E and F). These data, therefore, do not support the proposal that epiplakin plays a specific role in stabilizing keratin filament networks of simple epithelia.

DISCUSSION

Based on its strong expression in skin, in the outer cell layers in particular, epiplakin has been proposed to play an important role in epidermal barrier acquisition and function. This notion was supported by a report showing that trichohyalin, keratin, small prolin-rich protein, and involucrin are cross-linked to epiplakin in the inner root sheath of hair follicles (35) and by a recent study showing epiplakin interaction with keratins (17). However, our present study does not support this idea, as the

elimination of epiplakin by targeted inactivation of its gene in mice did not lead to any readily detectable defects in barrier function nor to any abnormalities of the hair coat. Epiplakin-deficient mice were viable and fertile, and a detailed phenotypic analysis of the skin did not reveal any abnormalities during embryonal development or dysfunctions in the adult state. This was unexpected, considering that mice lacking other members of the plakin protein family, such as plectin and BPAG1, did indeed show a skin phenotype.

On the other hand, null mutations in other plakins that are supposed to play a role in the outer epidermal layers such as envoplakin and periplakin did not reveal any severe phenotype either. Mice lacking envoplakin were shown to have only a slight delay in the acquisition of the epithelial barrier function and CE shape (23), while no abnormalities were reported for

periplakin-deficient mice (1). Moreover, mice deficient in other components of the CE, like involucrin or loricrin, were also shown to have no defects or only minor defects (6, 19). Similar to envoplakin$^{-/-}$ mice, differences in shape and integrity of CEs, as well as in the acquisition of the epithelial barrier function, were reported for loricrin$^{-/-}$ mice (19). Considering that no defects were detectable in epiplakin-deficient mice, it would have been conceivable that normal CE formation was achieved by compensatory mechanisms. However, investigating the protein levels of other plakins and/or CE components in epiplakin-deficient mice, we could not detect upregulation of any of these proteins. Thus, similar to ablations of periplakin, involucrin, and envoplakin, we obtained no evidence for any mechanisms compensating for the absence of epiplakin. Moreover, we did not observe stress marker expression (keratin 6) in the interfollicular epidermis, supporting the view that epiplakin-deficient skin is intact and unaffected.

On the cellular level, effects of plakin deficiency on cytoarchitecture have been reported in a number of cases. Perturbations of the keratin filament network have been found in desmoplakin$^{-/-}$ mice (11), and shorter and less stable microtubules have been reported in neurons of BPAG1 null mice (40). In the case of ACF7 ablation, microtubules appeared to be longer and less stable, and they displayed irregular cytoplasmic trajectories and alterations in their dynamic instability behavior (20). Plectin-deficient keratinocytes showed an increased number of vinculin-positive focal adhesion contacts, while the number of stable anchoring contacts was reduced in such cells (2). Furthermore, there is evidence that plectin is involved in the regulation of microtubule dynamics during stratification (unpublished data). In contrast, in the case of epiplakin, we found no difference between +/+ and -/- keratinocytes regarding cytoskeletal filament organization, including actin stress fibers, microtubules, and, particularly noteworthy, keratins. This was of interest especially in light of a recent report showing that epiplakin binds to keratins (17). The observed integrity of keratin networks in epidermal epiplakin$^{-/-}$ keratinocytes was in agreement with RNAi-mediated knockdown experiments of epiplakin in epidermal cell lines, which showed no effects on keratin filament organization (17). On the other hand, in HeLa cells epiplakin depletion by RNAi was reported to cause a collapse of keratin filaments, which led the authors to propose a more important function for epiplakin in simple epithelia, compared to stratified epithelia (17). However, monitoring keratin filament network organization in simple epithelia (small intestine and liver) of epiplakin-deficient mice, we could not find any alterations compared to wild-type mice. Furthermore, keratin filament organization in primary hepatocytes isolated from epiplakin$^{-/-}$ mice appeared normal. As epiplakin-deficient mice did not display any growth retardation compared to wild-type mice (data not shown), it seemed unlikely that simple epithelia of the digestive tract had any defects. Nevertheless, future functional analyses of tissues like small intestine, pancreas, or liver from epiplakin-deficient mice using organ-specific injury models may lead to a better understanding of epiplakin's role in such tissues.

In conclusion, we have shown that the absence of epiplakin does not have any severe consequences for vital functions of the mouse organism. Especially in skin, where epiplakin is abundantly expressed (33), an in-depth phenotypic analysis did not reveal any defects in the functions of this tissue. Surprisingly, despite epiplakin's putative 16 keratin-binding domains that would make the protein perfectly suited to act as a scaffold orchestrating keratin filament organization, intermediate filament networks seemed unaffected by epiplakin deficiency, as demonstrated for simple and stratified epithelia as well as cultured keratinocytes and hepatocytes. A possible involvement of epiplakin as a platform in signaling pathways, similar to plectin (25), has still to be investigated. In particular, epiplakin$^{-/-}$ cell lines will provide a powerful tool for studying the effects of epiplakin deficiency on signaling cascades.

REFERENCES

1. **Aho, S., K. Li, Y. Ryoo, C. McGee, A. Ishida-Yamamoto, J. Uitto, and J. F. Klement.** 2004. Periplakin gene targeting reveals a constituent of the cornified cell envelope dispensable for normal mouse development. Mol. Cell. Biol. **24:**6410–6418.
2. **Andrä, K., I. Kornacker, A. Jörgl, M. Zörer, D. Spazierer, P. Fuchs, I. Fischer, and G. Wiche.** 2003. Plectin-isoform-specific rescue of hemidesmosomal defects in plectin (−/−) keratinocytes. J. Investig. Dermatol. **120:**189–197.
3. **Andrä, K., H. Lassmann, R. Bittner, S. Shorny, R. Fässler, F. Propst, and G. Wiche.** 1997. Targeted inactivation of plectin reveals essential function in maintaining the integrity of skin, muscle, and heart cytoarchitecture. Genes Dev. **11:**3143–3156.
4. **Barel, A. O., and P. Clarys.** 1995. Study of the stratum corneum barrier function by transepidermal water loss measurements: comparison between two commercial instruments: Evaporimeter and Tewameter. Skin Pharmacol. **8:**186–195.
5. **Brown, A., G. Bernier, M. Mathieu, J. Rossant, and R. Kothary.** 1995. The mouse dystonia musculorum gene is a neural isoform of bullous pemphigoid antigen 1. Nat. Genet. **10:**301–306.
6. **Djian, P., K. Easley, and H. Green.** 2000. Targeted ablation of the murine involucrin gene. J. Cell Biol. **151:**381–388.
7. **Dreher, F., A. Arens, J. J. Hostynek, S. Mudumba, J. Ademola, and H. I. Maibach.** 1998. Colorimetric method for quantifying human Stratum corneum removed by adhesive-tape stripping. Acta Derm. Venereol. **78:**186–189.
8. **Eferl, R., M. Sibilia, F. Hilberg, A. Fuchsbichler, I. Kufferath, B. Guertl, R. Zenz, E. F. Wagner, and K. Zatloukal.** 1999. Functions of c-Jun in liver and heart development. J. Cell Biol. **145:**1049–1061.
9. **Eger, A., A. Stockinger, G. Wiche, and R. Foisner.** 1997. Polarisation-dependent association of plectin with desmoplakin and the lateral submembrane skeleton in MDCK cells. J. Cell Sci. **110:**1307–1316.
10. **Fujiwara, S., N. Takeo, Y. Otani, D. A. Parry, M. Kunimatsu, R. Lu, M. Sasaki, N. Matsuo, M. Khaleduzzaman, and H. Yoshioka.** 2001. Epiplakin, a novel member of the Plakin family originally identified as a 450-kDa human epidermal autoantigen. Structure and tissue localization. J. Biol. Chem. **276:**13340–13347.
11. **Gallicano, G. I., P. Kouklis, C. Bauer, M. Yin, V. Vasioukhin, L. Degenstein, and E. Fuchs.** 1998. Desmoplakin is required early in development for assembly of desmosomes and cytoskeletal linkage. J. Cell Biol. **143:**2009–2022.
12. **Guo, L., L. Degenstein, J. Dowling, Q. C. Yu, R. Wollmann, B. Perman, and E. Fuchs.** 1995. Gene targeting of BPAG1: abnormalities in mechanical strength and cell migration in stratified epithelia and neurologic degeneration. Cell **81:**233–243.
13. **Hashimoto, T., M. Amagai, T. Ebihara, S. Gamou, N. Shimizu, T. Tsubata,**

A. Hasegawa, K. Miki, and T. Nishikawa. 1993. Further analyses of epitopes for human monoclonal anti-basement membrane zone antibodies produced by stable human hybridoma cell lines constructed with Epstein-Barr virus transformants. J. Investig. Dermatol. **100:**310–315.

14. **Hennings, H.** 1994. Primary culture of keratinocytes from newborn mouse epidermis in medium with lowered levels of Ca2+, p. 21–23. *In* I. M. Leigh and F. M. Watt (ed.), Keratinocyte methods. Cambridge University Press, Cambridge, United Kingdom.

15. **Hogan, B., R. Beddington, F. Constantini, and E. Lacy.** 1994. Manipulating the mouse embryo: a laboratory manual. Cold Spring Harbor Laboratory Press, Cold Spring Harbor, N.Y.

16. **Hutter, H., K. Zatloukal, G. Winter, C. Stumptner, and H. Denk.** 1993. Disturbance of keratin homeostasis in griseofulvin-intoxicated mouse liver. Lab. Investig. **69:**576–582.

17. **Jang, S. I., A. Kalinin, K. Takahashi, L. N. Marekov, and P. M. Steinert.** 2005. Characterization of human epiplakin: RNAi-mediated epiplakin depletion leads to the disruption of keratin and vimentin IF networks. J. Cell Sci. **118:**781–793.

18. **Jefferson, J. J., C. L. Leung, and R. K. Liem.** 2004. Plakins: goliaths that link cell junctions and the cytoskeleton. Nat. Rev. Mol. Cell Biol. **5:**542–553.

19. **Koch, P. J., P. A. de Viragh, E. Scharer, D. Bundman, M. A. Longley, J. Bickenbach, Y. Kawachi, Y. Suga, Z. Zhou, M. Huber, D. Hohl, T. Kartasova, M. Jarnik, A. C. Steven, and D. R. Roop.** 2000. Lessons from loricrin-deficient mice: compensatory mechanisms maintaining skin barrier function in the absence of a major cornified envelope protein. J. Cell Biol. **151:**389–400.

20. **Kodama, A., I. Karakesisoglou, E. Wong, A. Vaezi, and E. Fuchs.** 2003. ACF7: an essential integrator of microtubule dynamics. Cell **115:**343–354.

21. **Laemmli, U. K.** 1970. Cleavage of structural proteins during the assembly of the head of bacteriophage T4. Nature **227:**680–685.

22. **Langhofer, M., S. B. Hopkinson, and J. C. Jones.** 1993. The matrix secreted by 804G cells contains laminin-related components that participate in hemidesmosome assembly in vitro. J. Cell Sci. **105:**753–764.

23. **Määttä, A., T. DiColandrea, K. Groot, and F. M. Watt.** 2001. Gene targeting of envoplakin, a cytoskeletal linker protein and precursor of the epidermal cornified envelope. Mol. Cell. Biol. **21:**7047–7053.

24. **Moll, R., W. W. Franke, D. L. Schiller, B. Geiger, and R. Krepler.** 1982. The catalog of human cytokeratins: patterns of expression in normal epithelia, tumors and cultured cells. Cell **31:**11–24.

25. **Osmanagic-Myers, S., and G. Wiche.** 2004. Plectin-RACK1 (receptor for activated C kinase 1) scaffolding: a novel mechanism to regulate protein kinase C activity. J. Biol. Chem. **279:**18701–18710.

26. **Reipert, S., I. Fischer, and G. Wiche.** 2004. High-pressure cryoimmobilization of murine skin reveals novel structural features and prevents extraction artifacts. Exp. Dermatol. **13:**419–425.

27. **Rice, R. H., and H. Green.** 1979. Presence in human epidermal cells of a soluble protein precursor of the cross-linked envelope: activation of the cross-linking by calcium ions. Cell **18:**681–694.

28. **Röper, K., S. L. Gregory, and N. H. Brown.** 2002. The "Spectraplakins": cytoskeletal giants with characteristics of both spectrin and plakin families. J. Cell Sci. **115:**4215–4225.

29. **Rothnagel, J. A., T. Seki, M. Ogo, M. A. Longley, S. M. Wojcik, D. S. Bundman, J. R. Bickenbach, and D. R. Roop.** 1999. The mouse keratin 6 isoforms are differentially expressed in the hair follicle, footpad, tongue and activated epidermis. Differentiation **65:**119–130.

30. **Ruhrberg, C., M. A. Hajibagheri, D. A. Parry, and F. M. Watt.** 1997. Periplakin, a novel component of cornified envelopes and desmosomes that belongs to the plakin family and forms complexes with envoplakin. J. Cell Biol. **139:**1835–1849.

31. **Sambrook, J., and Russell, D. W.** 2001. Molecular cloning: a laboratory manual, 3rd ed. Cold Spring Harbor Laboratory Press, Cold Spring Harbor, N.Y.

32. **Schmuth, M., G. Yosipovitch, M. L. Williams, F. Weber, H. Hintner, S. Ortiz-Urda, K. Rappersberger, D. Crumrine, K. R. Feingold, and P. M. Elias.** 2001. Pathogenesis of the permeability barrier abnormality in epidermolytic hyperkeratosis. J. Investig. Dermatol. **117:**837–847.

33. **Spazierer, D., P. Fuchs, V. Pröll, L. Janda, S. Oehler, I. Fischer, and G. Wiche.** 2003. Epiplakin gene analysis in mouse reveals a single exon encoding a 725-kDa protein with expression restricted to epithelial tissues. J. Biol. Chem. **278:**31657–31666.

34. **Steinert, P. M.** 2000. The complexity and redundancy of epithelial barrier function. J. Cell Biol. **151:**F5–F8.

35. **Steinert, P. M., D. A. Parry, and L. N. Marekov.** 2003. Trichohyalin mechanically strengthens the hair follicle: multiple cross-bridging roles in the inner root sheath. J. Biol. Chem. **278:**41409–41419.

36. **Uitto, J., and G. Richard.** 2004. Progress in epidermolysis bullosa: genetic classification and clinical implications. Am. J. Med. Genet. C **131C:**61–74.

37. **Wiche, G., and M. A. Baker.** 1982. Cytoplasmic network arrays demonstrated by immunolocalization using antibodies to a high molecular weight protein present in cytoskeletal preparations from cultured cells. Exp. Cell Res. **138:**15–29.

38. **Wiche, G., R. Krepler, U. Artlieb, R. Pytela, and H. Denk.** 1983. Occurrence and immunolocalization of plectin in tissues. J. Cell Biol. **97:**887–901.

39. **Wickett, R. R., V. Nath, R. Tanaka, and S. B. Hoath.** 1995. Use of continuous electrical capacitance and transepidermal water loss measurements for assessing barrier function in neonatal rat skin. Skin Pharmacol. **8:**179–185.

40. **Yang, Y., C. Bauer, G. Strasser, R. Wollman, J. P. Julien, and E. Fuchs.** 1999. Integrators of the cytoskeleton that stabilize microtubules. Cell **98:**229–238.